Electronic Supplementary Material (ESI) for ChemComm.

Super water–stable europium-organic framework: guests inducing low-humidity proton conduction and sensing of metal ions

Rui Wang,[a] Xi-Yan Dong,[a,b] Hong Xu,[a] Ru-Bo Pei, [a] Ming-Li Ma,[a] Shuang-Quan Zang,*[a] Hong-Wei Hou[a] and Thomas C. W. Mak [a,c]

[a] College of Chemistry and Molecular Engineering, Zhengzhou University, Zhengzhou 450001, China

[b] School of Physics and Chemistry, Henan Polytechnic University, Jiaozuo 454000, China

[c] Department of Chemistry and Center of Novel Functional Molecules, The Chinese University of Hong Kong, Shatin, New Territories, Hong Kong SAR, China

Author for correspondence: **Prof. Dr. S.-Q. Zang**

Supporting Information

Section S1: The arrangement of dimethylammonium cations

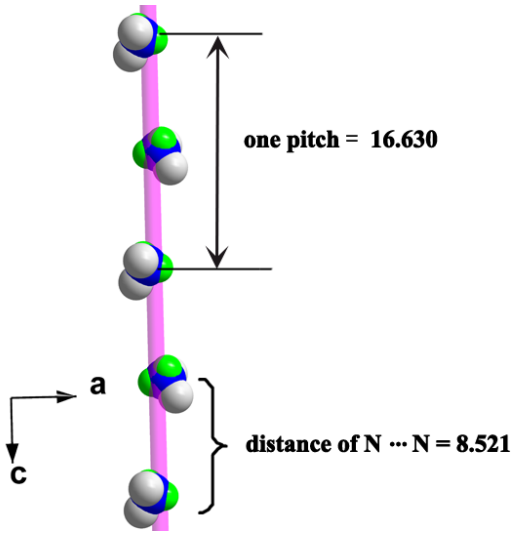

Fig. S1 The arrangement of dimethylammonium cations in the second larger channel. Distances are in angstrom (Å).

Section S2: Water Vapor Sorption

The as-made Eu-MOF was soaked in anhydrous methanol for 8 h. The supernatant was decanted and replenished four times over three days. A completely desolvated sample of about 100 mg was obtained by heating the solvent-exchanged bulk at 80 °C under dynamic high vacuum for 24 h. Water adsorption isotherms of the dehydrated Eu-MOF were measured on a Quantachrome IQ2 system. Before the water vapor measurement, the samples were evacuated again by using the "degas" function of the surface area analyzer for 10 h at 80 °C.

The dehydrated Eu-MOF retained the original structure, which has been approved by its indentical PXRD pattern with that of as-made Eu-MOF (Fig. S2).

The drastic increase of adsorbed water in the low vapor pressure range (0 – 30% RH) suggested that the water molecules are adsorbed in the pores of the materials. The amounts adsorbed water molecules are determined to be 3.0 (at 40 % RH) per $[Eu_2(L)_2]$ unit for Eu-MOF, which is compared to initial water content of Eu-MOF. Above that, adsorbed water continues gradually increasing. There is a small hysteresis in the adsorption/desorption process at low humidity (Fig. S3).

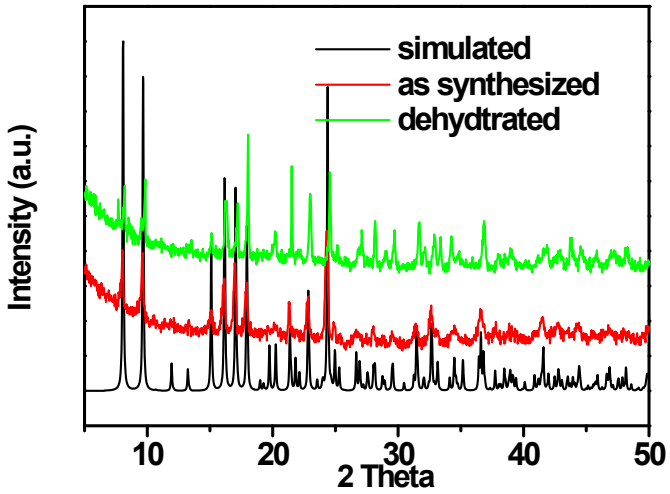

Fig. S2 PXRD patterns of simulated from single-crystal X-ray diffraction results, the as-synthesized and dehydrated **Eu-MOF**.

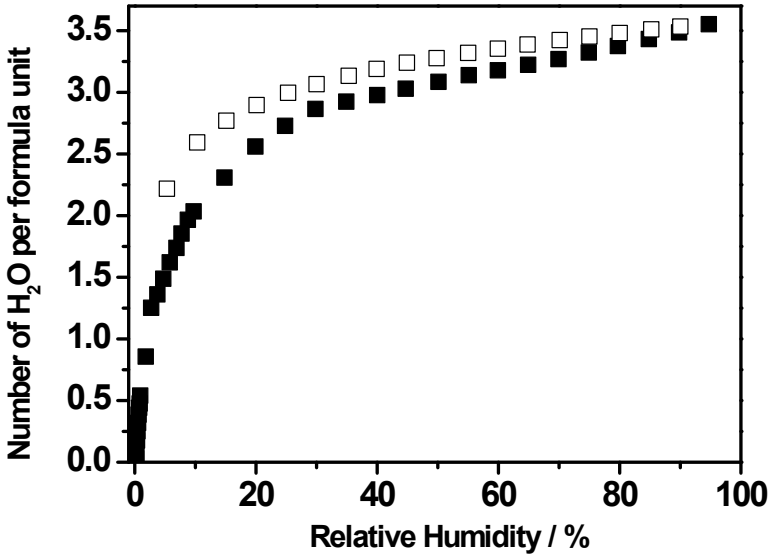

Fig. S3 Water vapor adsorption/desorption isotherms of the dehydrated **Eu-MOF** at 298 K. Closed and open squares correspond to the adsorption and desorption processes, respectively.

Section S3: Proton conductivity studies of Eu-MOF.

Method for measuring ionic/proton conductivity is impedance spectroscopy, in which a sinusoidally varying voltage is applied across the sample of interest, and the current flowing through the sample is measured as a function of the sinusoidal frequency. The complex impedance (Z) is then calculated by dividing the complex voltage by the complex current, as a function of frequency. A typical model for ion/proton transport through a grain of powdered material is the parallel combination of a resistor and capacitor, which in the frequency domain (after applying the Laplace transform) traces out a semicircle in the complex (Z'' vs Z') plane as a function of frequency. The conductivity of the sample is then calculated by geometrically scaling the low frequency intercept of the semicircle with the Z' (real) axis. So a typical impedance plot (Z'' vs Z') of ionic-conducting materials shows a semicircle in the high frequency region and a tail at low frequencies. The tail at low frequencies indicates blocking of protons at either the electrode or grain boundaries.

Proton conductivity was measured on the powdered crystalline samples Pellets. Ac impedance spectroscopy measurement was performed on a PARSTAT 2273 impedance analyzer over a frequency range from 0.1 Hz to 1 MHz, with a quasi-four-probe electrochemical cell and an applied ac voltage of 10 mV with copper electrodes (the purity of Cu is more than 99.9 %). The conductivity was calculated as $\sigma = (1/R)(h/S)$, where R is the resistance, h is the thickness, and S is the area of the tablet. Activation energies (Ea) were calculated by fitting the conductivity data to the Arrhenius relation for thermally activated conduction, which is given as $\sigma T = \sigma_0 \exp(-Ea / kT)$, where σ, σ_0, Ea, k, T are the conductivity, pre-exponential factor, activation energy, Boltzmann constant and absolute temperature, respectively.

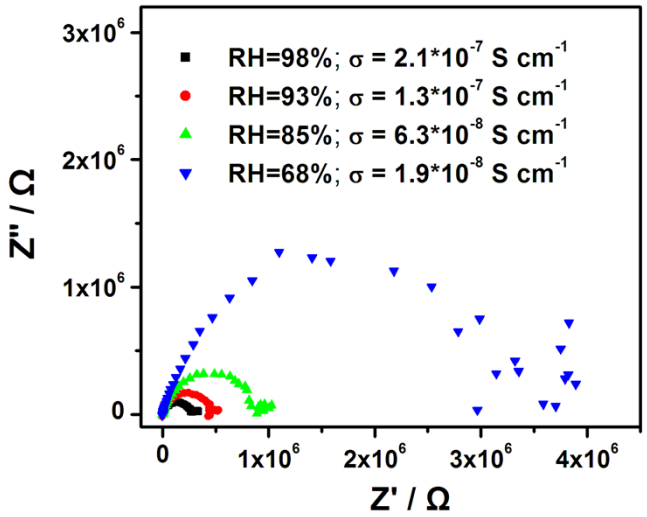

Fig. S4 Nyquist plots for **Eu-MOF** at room temperature and various relative humidity.

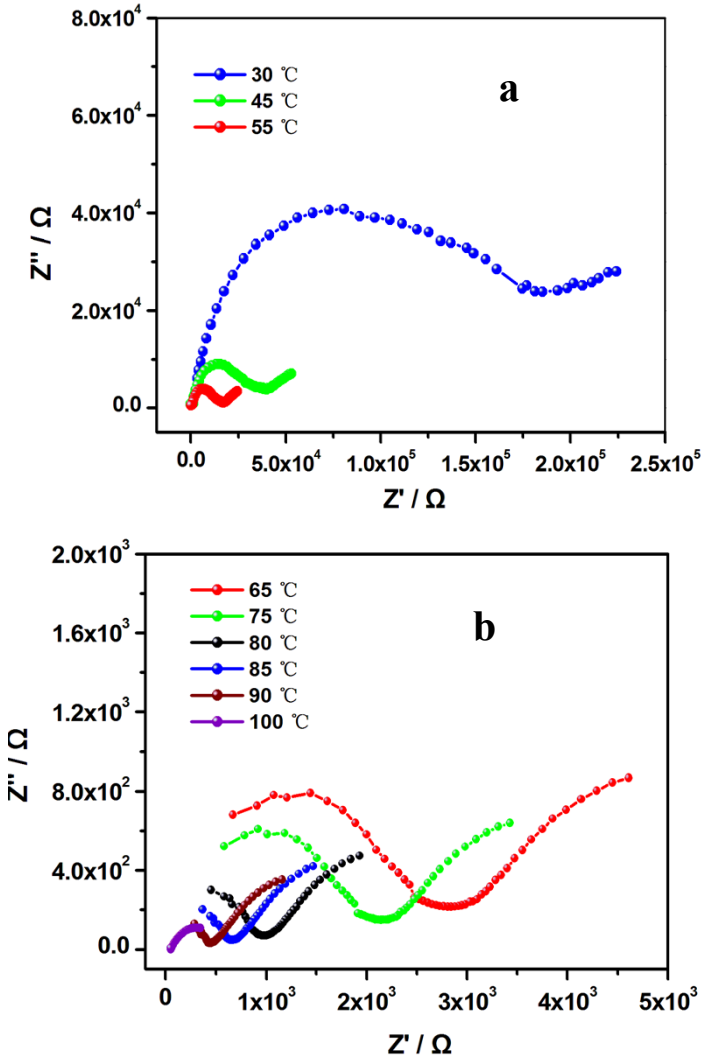

Fig. S5 Nyquist plots for **Eu-MOF** at 68% relative humidity and different temperature (a) 30–55 °C (b) 65–100 °C.

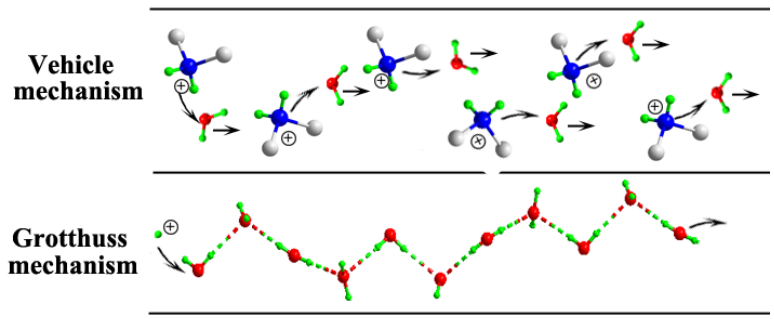

Fig. S6 The possible mechanisms of proton transport in **Eu-MOF**.

Table S1: Compare proton conductivity of CPs or MOFs containing dimethyl ammonium and other proton-conducitng MOFs reported in the last two years with that of **Eu-MOF** in this work.

Compound	Pore guests	σ / S cm^{-1}	RH %	T (^{o}C)	Water satbility	Published year
Eu-MOF	**$[H_2N(CH_3)_2]^+$, water**	**1.1×10^{-3}**	**98**	**100**	**Yes**	**This work**
Cd-5TIA[1]	$[H_2N(CH_3)_2]^+$	3.6×10^{-3}	98	28	—[a]	2012
In-5TIA[1]	$[H_2N(CH_3)_2]^+$	5.35×10^{-5}	98	28	—	2012
In-IA-2D-1[2]	$[H_2N(CH_3)_2]^+$, water	3.4×10^{-3}	98	27	—	2013
In-IA-2D-2[2]	$[H_2N(CH_3)_2]^+$, DMF	1.59×10^{-5}	anhydrous	120	—	2013
$[(CH_3)_2NH_2][Zn_3Na_2(cpida)_3]\cdot2.5DMF$[3]	$[H_2N(CH_3)_2]^+$, absorbed H_2O	2.1×10^{-6}	97	95		2013
$\{[(Me_2NH_2)_3(SO_4)]_2[Zn_2(ox)_3]\}_n$[4]	$[H_2N(CH_3)_2]^+$and SO_4^{2-}	4.2×10^{-2}	98	ambient room	Yes	2014
		1×10^{-4}	anhydrous	150		
$[Zn_3(5\text{-sip})_2(5\text{-sipH})(bpy)]\cdot(DMF)\cdot2(DMA)$[5]	$[H_2N(CH_3)_2]^+$, DMF	8.7×10^{-5}	60	25	—	2014
$(NBu_4$-ZIF-8-OH)[6]	OH^-	2.3×10^{-8}	99	25		2014
CaPiPhtA-NH_3[7]	Lattice water, NH_3	6.6×10^{-3}	98	24	—	2014
$(NH_4)_2(adp)[Zn_2(ox)_3]\cdot3H_2O$[8]	NH_{4+}, Lattice water	8×10^{-3}	100	25	—	2014
$(NH_4)_5[Mn^{II}2Cr^{III}3(ox)_9]\cdot10H_2O$[9]	NH_{4+}, Lattice water	7.1×10^{-4}	74	25	No	2014
$[EuL(H_2O)_3]\cdot2H_2O$[9]	Uncoordinated pore water	1.6×10^{-5}	97	75	—	2014
$[DyL(H_2O)_3]\cdot2H_2O$[9]		1.33×10^{-5}				
$[Zn(H_2PO_4)_2(HPO_4)]\cdot(H_2dmbim)_2$[10]	$H_2PO_4^-$ and HPO_4^{2-}	2×10^{-4}	anhydrous	190	Yes	2014
$\{[Cd_2(L)_3(DMF)(NO_3)](DMF)_3(H_2O)_8\}_n$[11]	DMF, Lattice water	1.3×10^{-5}	98	25	—	2014
$[H_3O][Mn_3(\mu_3\text{-}OH)(C_{14}H_8O_6S)_3(H_2O)](DMF)_5$[12]	H_3O+, DMF, water	3×10^{-4}	98	34	—	2014
PCMOF-5[13]	Free phosphonic acid groups and water lining 1D pores	2.5×10^{-3}	98	60.1	Yes	2013
$\{NMe_3(CH_2COOH)\}[FeCr(ox)_3]\cdot3H_2O$[14]	Lattice water	8×10^{-5}	65	25	—	2012
Et−MnCr[14]		2×10^{-4}	80			
Bu-FeCr[14]		5×10^{-6}	90			
Bu-MnCr[14]		9×10^{-8}				
Et−FeCr·$2H_2O$[15]	Lattice water	10^{-7}	65	25	No	2013

Et−FeFe·2H_2O[15]						
$[Zn_3(H_2PO_4)_6](Hbim)$[16]	Benzimidazole	1.3×10^{-3}	anhydrous	120	—	2013
$[Zn_3(H_2PO_4)_6(H_2O)_3](Hbim)$[16]		6.1×10^{-7}	anhydrous	60	—	2013
$ZrF[H_3(O_3PCH_2NHCH_2COO)_2]$[17]	Hydrogen bonding between carboxylic acid groups on adjacent chains	1×10^{-3}	95	140	—	2013
$Mn^{II}3[Nb^{IV}(CN)_8]_2$(4-aminopyridine)$_{10}$(4-aminopyridinium)2·12$H_2O$[18]	4-NH_2pyH^+ and water	4.6×10^{-4}	100	49	—	2013
Cu-DSOA	H_3O^+ and water	1.9×10^{-3}	98	85	Yes	2013

[a] The water stability of compounds has not been investigated in paper.

References:

[1] T. Panda,T, Kundu and R, Banerjee, *Chem. Commun.*, 2012, **48**, 5464–5466.

[2] T. Panda, T. Kundu and R. Banerjee, *Chem. Commun.*, 2013, **49**, 6197–6199.

[3] X. Meng, X.-Z. Song, S.-Y. Song, G.-C. Yang, M. Zhu, Z.-M. Hao, S.-N. Zhao and H.-J. Zhang, *Chem. Commun.*, 2013, **49**, 8483–8485.

[4] S. S. Nagarkar, S. M. Unni, A. Sharma, S. Kurungot and S. K. Ghosh, *Angew. Chem. Int. Ed.*, 2014, **53**, 2638–2642.

[5] P. Ramaswamy, R. Matsuda, W. Kosaka, G. Akiyama, H. Joon Jeona and S. Kitagawa, *Chem. Commun.*, 2014, **50**, 1144–1146.

[6] M. Sadakiyo, H. Kasai, K. Kato, M. Takata and M. Yamauchi, *J. Am. Chem. Soc.*, 2014, **136**, 1702–1705.

[7] M. Bazaga-García, R. M. P. Colodrero, M. Papadaki, P. Garczarek, J. Zoń, P. Olivera-Pastor, E. R. Losilla, L. León-Reina, M. A. G. Aranda, D. Choquesillo-Lazarte, K. D. Demadis and A. Cabeza, *J. Am. Chem. Soc.*, 2014, **136**, 5731−5739.

[8] (a) M. Sadakiyo, T. Yamada, K. Honda, H. Matsui and H. Kitagawa, *J. Am. Chem. Soc.*, 2014, **136**, 7701–7707; (b) M. Sadakiyo, T. Yamada, H. Kitagawa, *J. Am. Chem. Soc.*, 2009, **131**, 9906–9907.

[9] M. Zhu, Z.-M. Hao, X.-Z. Song, X. Meng, S.-N. Zhao, S.-Y. Song and H.-J. Zhang, *Chem. Commun.*, 2014, **50**, 1912–1914.

[10] M. Inukai, S. Horike, W. Chen, D. Umeyama, T. Itakura and S. Kitagawa, *J. Mater. Chem. A*, 2014, DOI: 10.1039/C4TA01261E.

[11] S. Sen, T. Yamada, H. Kitagawa and P. K. Bharadwaj, *Cryst. Growth Des.*, 2014, **14**, 1240−1244.

[12] S. Bhattacharya, M. Gnanavel, A. J. Bhattacharyya and S. Natarajan, *Cryst. Growth Des.*, 2014, **14**, 310–325.

[13] J. M. Taylor, K. W. Dawson and G. K. H. Shimizu, *J. Am. Chem. Soc.*, 2013, **135**, 1193–1196.

[14] M. Sadakiyo, H. Ōkawa, A. Shigematsu, M. Ohba, T. Yamada and H. Kitagawa, *J. Am.*

Chem. Soc., 2012, **134**, 5472−5475.
[15] H. Ōkawa, M. Sadakiyo, T. Yamada, M. Maesato, M. Ohba and H. Kitagawa, *J. Am. Chem. Soc.*, 2013, **135**, 2256−2262.
[16] D. Umeyama, S. Horike, M. Inukai and S. Kitagawa, *J. Am. Chem. Soc.*, 2013, **135**, 11345–11350.
[17] M. Taddei, A. Donnadio, F. Costantino, R. Vivani and M. Casciola, *Inorg. Chem.*, 2013, **52**, 12131−12139.
[18] K. Imoto, K. Nakagawa, H. Miyahara and S. Ohkoshi, *Cryst. Growth Des.*, 2013, **13**, 4673–4677.
[19] X.-Y. Dong, R. Wang, J.-B. Li, S.-Q. Zang, H.-W. Hou and T. C. W. Mak, *Chem. Commun.*, 2013, **49**, 10590–10592.

Section S4: Studies of sensing metal ions through cation exchange

4.1 Detailed ion-exchange experiments of Eu-MOF are as follows:

The as-synthesized Eu-MOF crystals of 40 mg dispersed in 0.01 mol L^{-1} aqueous solution containing $M(NO_3)_x$ (M = Li^+, Na^+, K^+, Ag^+, Mg^{2+}, Ca^{2+}, Ba^{2+}, Cr^{3+}, Mn^{2+}, Fe^{2+}, Fe^{3+}, Co^{2+}, Ni^{2+}, Cu^{2+}, Zn^{2+} and Pb^{2+}) for 3 days to form M^{n+}@Eu-MOF, which are then filtered and washed with fresh distilled water for many times till the filtrate is completely colorless to wash off the cations physically absorbed on the surface of the crystals. Next, M^{n+}@Eu-MOFs are dried in air for the sensing studies.

To further understand the process of cations exchange, we choose the concentration of 0.1 mol L^{-1} Fe^{3+}/Cu^{2+} aqueous solution for the next time-dependent experiments. The grounded powder samples of **Eu-MOF** has been introduced in Fe^{3+}/Cu^{2+} solution for different time (such as 5 min, 10 min, 30 min, 1 h, 2 h, 5 h, 1 d) to obtain time-dependent Fe^{3+}@Eu-MOF and Cu^{2+}@Eu-MOF samples, are then filtered and washed with fresh distilled water for many times till the filtrate is completely colorless to wash off the cations physically absorbed on the surface of the crystals. Next, these time-dependent Fe^{3+}@Eu-MOF and Cu^{2+}@Eu-MOF samples are dried in air. Then we analyzed time-dependent luminescence intensity, PXRD patterns, IR spectra, element analysis (EA) and ICP of solid sample Fe^{3+}/Cu^{2+}@Eu-MOF as well as ICP of their filtrate after "ion-exchanging".

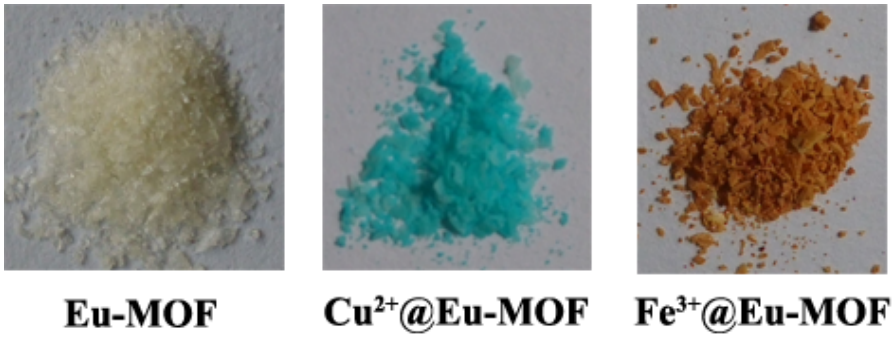

Fig. S7 Photographs of the Eu-MOF crystals, Cu^{2+}@Eu-MOF, and Fe^{3+}@Eu-MOF after

immersion in Cu^{2+}/Fe^{3+} aqueous solution.

4.2. Time-dependent luminescence of Fe^{3+}@Eu-MOFs and Cu^{2+}@Eu-MOFs.

The PL intensity of Cu^{2+}@Eu-MOFs after Cu^{2+} solution treating for 5 minutes decreased to 14% of that of pure Eu-MOF. The PL intensity of Fe^{3+}@Eu-MOFs after Fe^{3+} solution treating for 5 min decreased to about 26 % of that of pure Eu-MOF. With the exchange time increasing, the fluorescence intensity of Fe^{3+}@Eu-MOFs and Cu^{2+}@Eu-MOFs continue lessening.

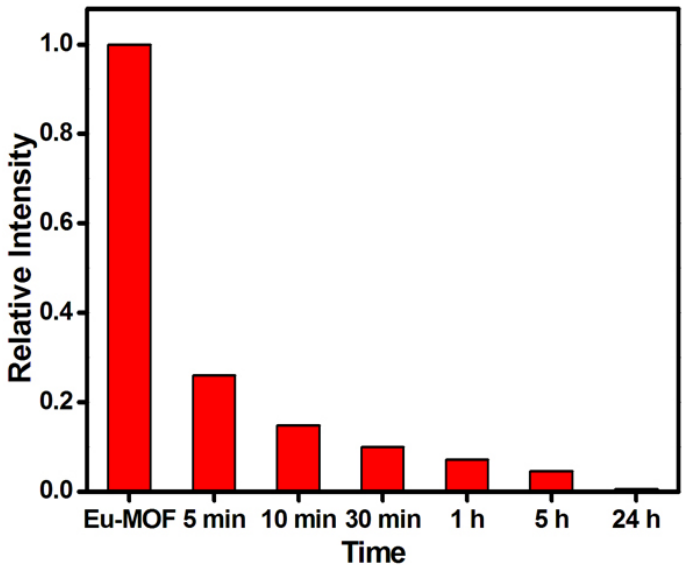

Fig. S8 The emission intensity of time-dependent of Fe^{3+}@Eu-MOF obtained after immersion in Fe^{3+} aqueous solution for different immersion time.

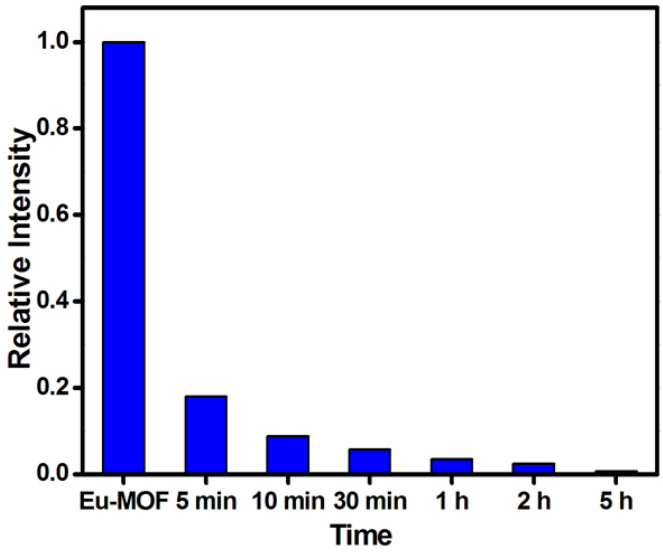

Fig. S9 The emission intensity of time-dependent Cu^{2+}@Eu-MOF obtained after immersion in Cu^{2+} aqueous solution for different immersion time.

4.3 Time-dependent Powder X-ray diffraction (PXRD) of Fe^{3+}@Eu-MOFs and Cu^{2+}@Eu-MOFs

For time-dependent Fe^{3+}@Eu-MOFs, the profile of the PXRD patterns did not show obvious variation in 10 minutes, indicating that the host framework of Eu-MOF retained before in 10 minutes in Fe^{3+} aqueous solution. And 30 minutes later, the diffraction intensity at 8.14° and 9.65° respectively in 2θ gradually decreased and finally disappeared (1d), and meanwhile new peaks at 14.26°, 15.46° of free liand (H_4L= 5-(3,5-dicarboxybenzyloxy)-isophthalic acid) started to appear more prominently suggesting the collapse of the original crystal structure and transformation to ligand (H_4L).

PXRD patterns of Cu^{2+}@Eu-MOF do not change with the immersion time and well match with the simulated pattern from single crystal Eu-MOF from beginning to end, suggesting the framework of Eu-MOF remains, although the photoluminescence is mostly quenched.

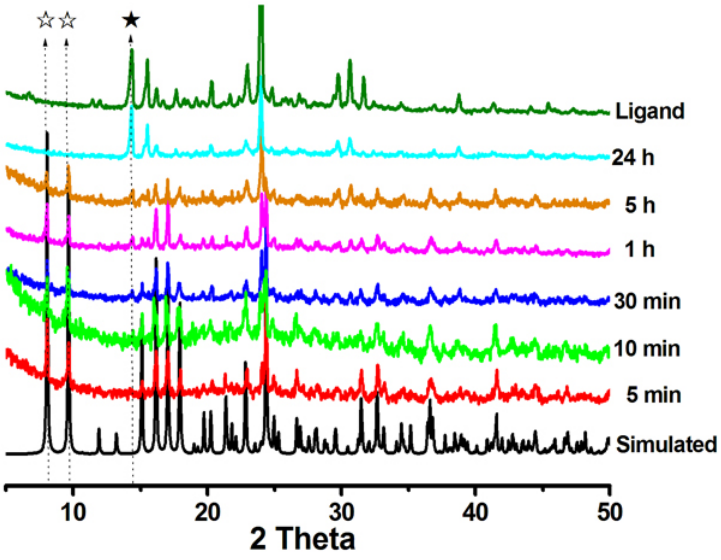

Fig. S10: PXRD patterns of time-dependent Fe^{3+}@Eu-MOF obtained after immersion in Fe^{3+} aqueous solution for different immersion time, free ligand (H_4L= 5-(3,5-dicarboxybenzyloxy) -isophthalic acid) and the simulated pattern of **Eu-MOF**.

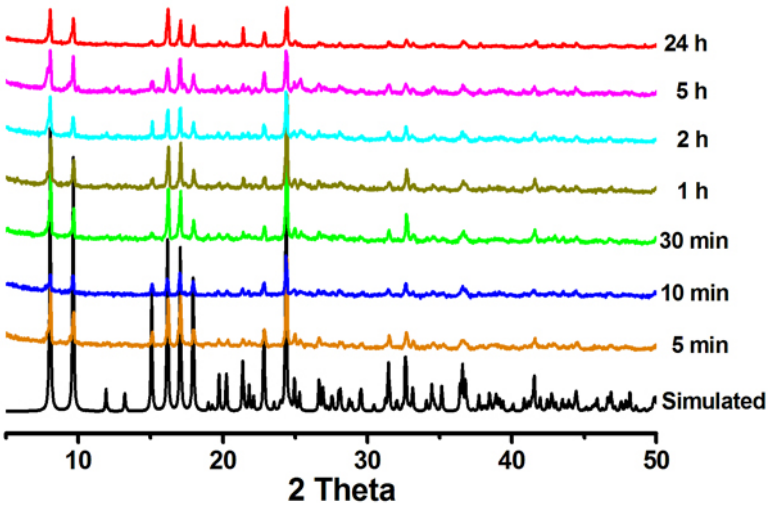

Fig. S11. PXRD patterns of time-dependent Cu^{2+}@Eu-MOF obtained after immersion in Cu^{2+} aqueous solution for different immersion time and the simulated pattern of **Eu-MOF**.

4.4 Time-dependent IR spectra of Fe^{3+}@Eu-MOFs and Cu^{2+}@Eu-MOFs

The adsorption band at 1700 cm^{-1} indicative of free carboxylic acid group[20] is not found in Cu^{2+}@Eu-MOFs and pure Eu-MOFs, but appeared in the IR profiles of Fe^{3+}@Eu-MOFs. The results suggest that some COO– groups are not coordinated to the metal ions and has been protonated in solid-state Fe^{3+}@Eu-MOFs.

References:

[20] (a) L.-R. Yang, S. Song, H.-M. Zhang, W. Zhang, L.-Z. Wu, Z.-W. Bu, T.-G. Ren, *Synthetic Metals* 2012, **162**, 261–267; (b) G. Majano, O. Ingold, M. Yulikov, G. Jeschkeb, J. Pérez-Ramírez, *CrystEngComm*, 2013, **15**, 9885–9892; c) L. J. Bellamy The Infrared Spectra of Complex Molecules. New York: Wiley, 1958

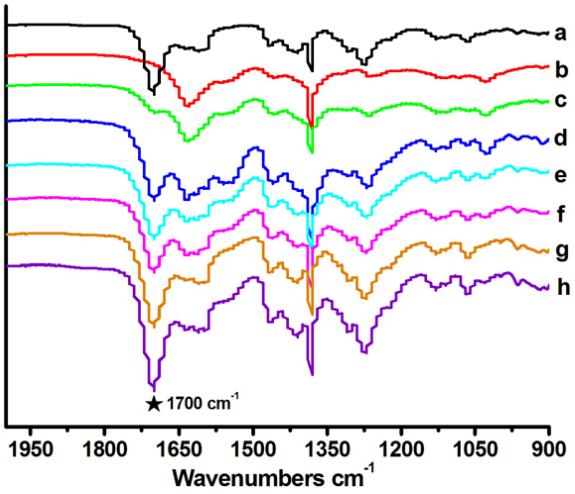

Fig. S12. IR spectra at room temperature. (a) free ligand (H_4L= 5-(3,5-dicarboxybenzyloxy)-isophthalic acid); (b) pure Eu-MOF and time-dependent Fe^{3+}@Eu-MOF: (c), (d), (e), (f), (g), (h) corresponding to 5 min, 10 min, 30 min, 1 h, 5 h, 24 h respectively.

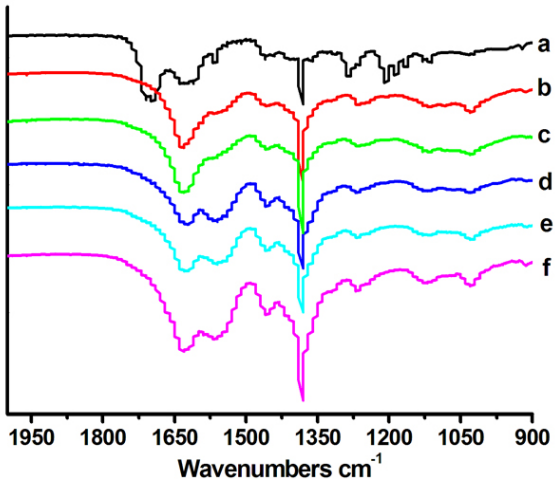

Fig. S13. IR spectra at room temperature. (a) free ligand (H_4L= 5-(3,5-dicarboxybenzyloxy)-isophthalic acid); (b) pure Eu-MOF and time-dependent Cu^{2+}@Eu-MOF: (c), (d), (e), (f) corresponding to 30 min, 1 h, 5 h, 24 h respectively.

4.5 Time-dependent Element Analysis and ICP analysis

Eu-MOF after immersion in aqueous solution containing different metal cations was filtered and then washed with fresh distilled water many times till the filtrate is completely colorless. The quantity of exchanged dimethylammonium cations can be evaluated by measuring the "N" content in time-dependent Element Analysis. Time-dependent ICP measurement can monitor the amount of Eu^{3+} and Cu^{2+}/Fe^{3+} in solid-state Cu^{2+}@Eu-MOF and Fe^{3+}@Eu-MOF obtained after immersion in Cu^{2+}/Fe^{3+} aqueous solution. ICP analysis of the filtrate at different ion-exchanging time is favorable to determine the Eu^{3+} content dissolved or exchanged with guests. The results of EA and ICP are listed as Table S2 and S3 respectively.

Time-dependent element analysis showed the $[H_2N(CH_3)_2]^+$ content in both Fe^{3+}@Eu-MOF and

Cu^{2+}@Eu-MOF decreased with immersion time increasing. Meanwhile, ICP analysis of the solid sample demonstrated Cu^{2+} content increased with the immersion time increasing and Fe^{3+} was slightly lifted in its solid sample in the measured time. Additionally, the Eu(III) content of the time-dependent filtrate after "Cu^{2+}-exchanging" is negligible little. In contrast, the Eu(III) content of the time-dependent filtrate after "Fe^{3+}-exchanging" continue increasing, which are attributed to the collapse of framework and Eu^{3+} dissolved in solution.

Table S2: Time-dependent EA (elemental analysis) and ICP results of Fe^{3+}@Eu-MOF obtained after immersion in Fe^{3+} aqueous solution, as well as ICP results of the time-dependent filtrate after "ion-exchanging".

N% in solid Fe^{3+}@Eu-MOF observed in EA results	$[(CH_3)_2NH_2]^+$ in solid Fe^{3+}@Eu-MOF calculated according to N content	Eu in solid sample Fe^{3+}@Eu-MOF	Fe in solid sample Fe^{3+}@Eu-MOF	Eu^{3+} ion amount (ppm) in filtrate after Fe^{3+} exchanging observed in ICP results	Immersion time in Fe^{3+} aqueous solution
1.63	5.37	17.01	1.07	6.66	5 min
1.25	4.11	16.28	1.69	14.48	10 min
0.92	3.02	11.53	1.21	15.97	30 min
0.88	2.89	11.52	1.38	18.1	1 h
0.58	1.91	10.89	1.75	18.22	5 h
0.09	0.29	6.17	3.29	21.26	24 h

Table S3. Time-dependent EA (elemental analysis) and ICP results of Cu^{2+}@Eu-MOF obtained after immersion in Cu^{2+} aqueous solution as well as ICP results of the time-dependent filtrate after ion-exchanging.

N content (%) in solid Cu^{2+}@Eu-MOF observed in EA results	$[(CH_3)_2NH_2]^+$(%) in solid Cu^{2+}@Eu-MOF calculated according to N% content	Eu in solid sample Cu^{2+}@Eu-MOF	Cu in solid sample Cu^{2+}@Eu-MOF	Eu^{3+} ion amount (ppm) filtrate after Cu^{2+} exchanging observed in ICP results	Immersion time in Cu^{2+} aqueous solution
1.52	5.13	16.81	1.83	0.34	5 min
1.35	4.44	16.46	2.47	0.39	10 min
1.14	3.75	15.78	3.08	0.43	30 min
1.18	3.88	15.19	3.33	0.47	1 h
1.13	3.71	14.98	4.33	0.53	2 h
0.93	3.06	14.54	5.45	0.72	5 h
0.84	2.76	13.87	6.38	0.95	24 h

4.6 The quenching effect of Eu-MOF as a function of Cu^{2+}, Fe^{3+} concentration

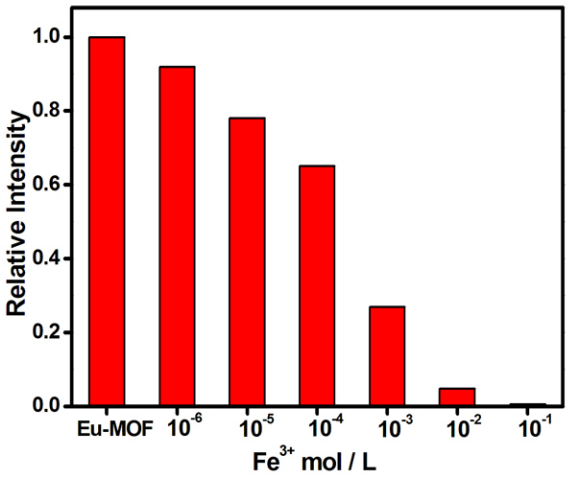

Fig. S14 Fluorescence intensity (at 616 nm) of Fe^{3+}@Eu-MOF solid sample after 24 h immersion as a function of $Fe(NO_3)_3$ concentration in solution, λ_{ex} = 320 nm.

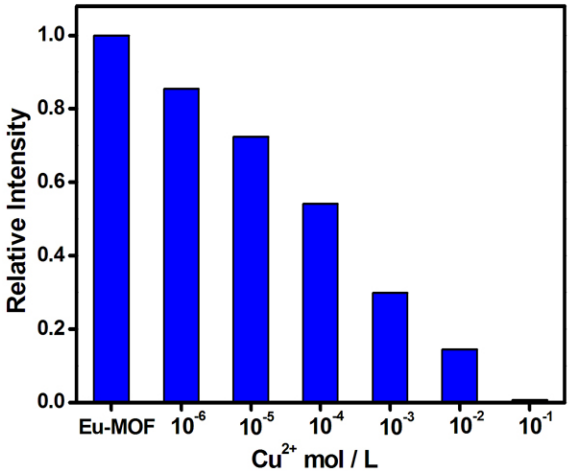

Fig. S15 Fluorescence intensity (at 616 nm) of Cu^{2+}@Eu-MOF solid sample after 5 h immersion as a function of $Cu(NO_3)_2$ concentration in solution, λ_{ex} = 320 nm.